

A Note on the Transient Electrohydrodynamics of a Liquid Drop

Asgar Esmaeeli¹ and Ali Behjatian¹

Abstract: The evolution of the flow field in and around a liquid drop in a uni-form electric field for fluid systems corresponding to region (II) of the circulation-deformation map is fundamentally different than that for the rest of the map and has not been explored before. This is examined here and justified mathematically. Furthermore a methodology is developed to predict the flow pattern, which is likely to be helpful in predicting the evolution of the flow field in more complex circumstances.

1 Introduction

This study is motivated by a recent computational simulations of Halim and Esmaeeli (2013) concerning the transient electrohydrodynamics of a two-dimensional liquid drop in a uniform electric field at low Reynolds and Ohnesorge numbers; $Re = \rho_o u_s a / \mu_o = 1$, $Oh = \mu_o / \sqrt{\rho_o a \gamma} = 0.5$, $u_s = \epsilon_o E_0^2 a / \mu_o$ and a being the electrohydrodynamic velocity scale and the drop radius. There we explored the behavior of a deformable liquid drop in a confined domain whose steady state deformation and flow pattern corresponded to one of the three regions of the circulation-deformation map (Fig. (2), to be discussed shortly) and observed that the final stage of the flow evolution toward steady state was the same for the cases that corresponded to regions (I) and (III) and distinctly different than those corresponding to region (II). For all the cases considered four vortices appeared in the domain (in a short period of time) that were crossing the surface of the drop and extending to the boundaries of the computational domain. However, whereas for the fluid systems corresponding to regions (I) and (III) these vortices gradually “retreated” from the drop, leaving behind four vortices inside the drop that grew to occupy the drop, for fluid systems corresponding to region (II) the vortices gradually “penetrated” into the drop until they were confined within the drop. As the focus of that study was mainly on the deformation-time history of the drop, these observations were not

¹ Southern Illinois University Carbondale

reported in that article. Interestingly, it turns out that the same is true for electrohydrodynamics of a three-dimensional liquid drops in an unbounded domain for creeping ($Re = \rho_o u_s a / \mu_o \ll 1$) and large Ohnesorge number squared ($Oh^2 \gg 1$) flows and that the observations can be justified using the analytical solution for these flows [Esmaeeli and Sharifi (2011)]. This is the goal of this study. This information will find relevance in a number of applications such as enhancement of chaotic mixing inside a drop by oscillatory-in-time electric field [Christov and Homsy (2009)].

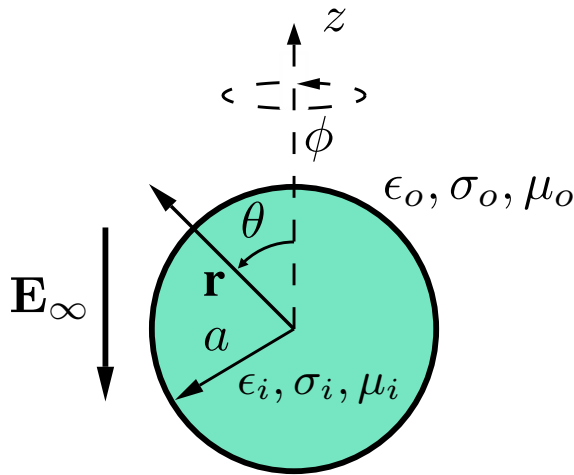


Figure 1: The Physical setup of the problem.

To put the work in perspective, we begin by providing a brief summary of the steady state and transient electrohydrodynamics of a liquid drop in a weak electric field in an unbounded domain [Fig. (1)] in the next two paragraphs.

The key parameters that control the senses of fluid flow and drop deformation are the ratios of the electric conductivity and permittivity of the drop fluid to the ambient fluid ($R = \sigma_i / \sigma_o$ and $S = \epsilon_i / \epsilon_o$, respectively). The sense of the fluid circulation in and around the drop at steady state is determined by the relative importance of R and S ; for $R > S$ the external flow at the surface of the drop runs from the equator to the poles, for $R < S$ the direction of the flow is reversed, and for $R = S$ the flow ceases to exist [Taylor (1966)]. The sense of drop deformation at steady state is determined by a characteristic parameter

$$\Phi = R^2 + 1 - 2S + \frac{3}{5}(R - S) \frac{3\tilde{\mu} + 2}{\tilde{\mu} + 1}, \quad (1)$$

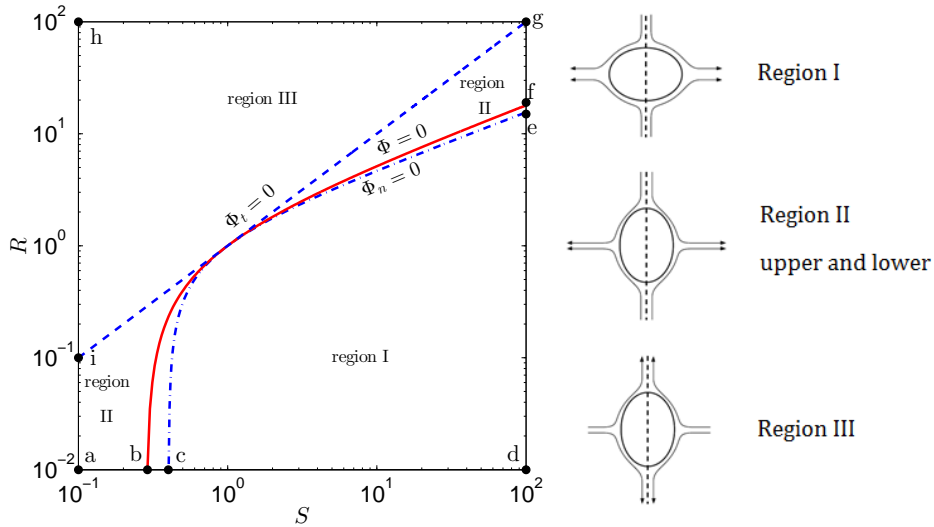


Figure 2: The circulation-deformation map along with the schematics of the steady state flow pattern (pole-to-equator vs. equator-to-pole) and modes of drop deformation (oblate vs. prolate) in each region. The direction of the electric field \mathbf{E}_∞ is downward. The internal circulation is not shown in the schematics.

$\tilde{\mu} = \mu_i/\mu_o$ being the viscosity ratio [Vizika and Saville (1992)]. For $\Phi > 0$ the drop becomes prolate (i.e., an ellipsoid with its major axis parallel to the direction of the electric field), for $\Phi < 0$ the drop becomes oblate (i.e., an ellipsoid with its major axis perpendicular to the direction of the electric field), and for $\Phi = 0$ the drop remains spherical. The steady-state electrohydrodynamics can be best described by considering the so-called circulation-deformation map [Fig. (2)]. This map is constructed by plotting the zero-circulation line [$\Phi_t \equiv R - S = 0$, dashed line] and the zero-deformation curve [$\Phi = 0$, solid line] in $S - R$ coordinates. This results in three regions: in region (I), confined between the $\Phi = 0$ curve and the lines \overline{bcd} and \overline{def} , the drop becomes oblate and the external flow at its surface runs from the poles toward the equator; in region (II), confined between the $\Phi = 0$ curve and the lines $\Phi_t = 0$, \overline{ia} , \overline{ab} , and \overline{fg} , the drop becomes prolate and the external flow at its surface runs from the poles toward the equator; and in region (III), confined between the $\Phi = 0$ and lines \overline{gh} and \overline{hi} , the drop becomes prolate and the external flow at its surface runs from the equator toward the poles.

The transient electrohydrodynamics of a drop in a weak electric field (i.e., $Re \ll 1$ and $Ca = \mu_o u_s/\gamma \ll 1$) and large Ohnesorge number squared ($Oh^2 \gg 1$) was studied by Esmaeli and Sharifi (2011) using a closed form analytical solution.

Here the dynamic is governed by only one characteristic time $\tau = [(19\tilde{\mu} + 16)(2\tilde{\mu} + 3)/(40\tilde{\mu} + 40)]t_s$, $t_s = \mu_o a / \gamma$ being the time scale of the drop deformation. The drop deforms monotonically and settles to its steady state deformation according to $\mathcal{D} = \mathcal{D}_\infty [1 - \exp(-t/\tau)]$, where the deformation parameter is defined as $\mathcal{D} = (z_{max} - r_{max}) / (z_{max} + r_{max})$, z_{max} and r_{max} being the end-to-end length of the drop in the direction of electric field and the maximum breadth in the traverse direction, respectively. The steady state deformation is $\mathcal{D}_\infty = (9Ca/16)[\Phi/(R+2)^2]$.

2 Evolution of the Flow Field

Having provided the essential background, we now explore the evolution of the flow field for representative fluid systems chosen from the three regions of the circulation-deformation map using the solution of Esmaeeli and Sharifi (2011). Figure (3) shows the evolution of the flow field (in a meridian plane) for a fluid system corresponding to region (III) at the selected times. Here, $R = 29.8$, $S = 2.27$, $\tilde{\mu} = 0.54$, and $Oh = 51.6$. The times are $t = 0, 3.5\tau$, and 8τ , where τ is the characteristic time of the problem Esmaeeli and Sharifi (2011). The steady state deformation parameter is $\mathcal{D} = 0.0023$. The fluid flow is established impulsively in and around the drop surface (frame *a*) since the time scale of momentum diffusion is much shorter than that of the drop deformation (i.e., $\partial \mathbf{u} / \partial t \ll 1$). As time passes, the extended vortices gradually retreat from the drop, leaving behind two toroidal vortices inside the drop in the upper and the lower hemispheres (frame *b*). Here the dashed-line marks the dividing streamline (separatrix) that separates the inner vortices from the original extended vortices. Further outward displacement of the extended vortices leads to the continuous growth of the inner vortices until they occupy the drop (frame *c*). At steady state, the separatrix resides at the surface of the drop and the steady state flow pattern is similar to the pertinent one depicted in Fig. (2). Furthermore, the drop deforms to a prolate.

The evolution of the flow field for a fluid system chosen from region (I) (not shown here) will be exactly the same as that shown in Fig. (3), except that the direction of the arrows will be the opposite, in line with the steady state sense of the flow [Fig. (2)]. On the other hand, for the fluid system chosen from region (II) the evolution of the flow field is diametrically opposite [Fig. (4)]. Here as before the flow is established impulsively and the initially extended vortices cross the drop. However, as time passes, the original extended vortices move gradually inward while the curvature of the streamlines that comprise the vortices continually increases (frame *b*). This transforms the open-ended vortices to closed vortices that are separated from a newly formed open-ended counterpart vortices by a dividing streamline. Here the scale of the figure obscures this development to be seen in frame (*b*).

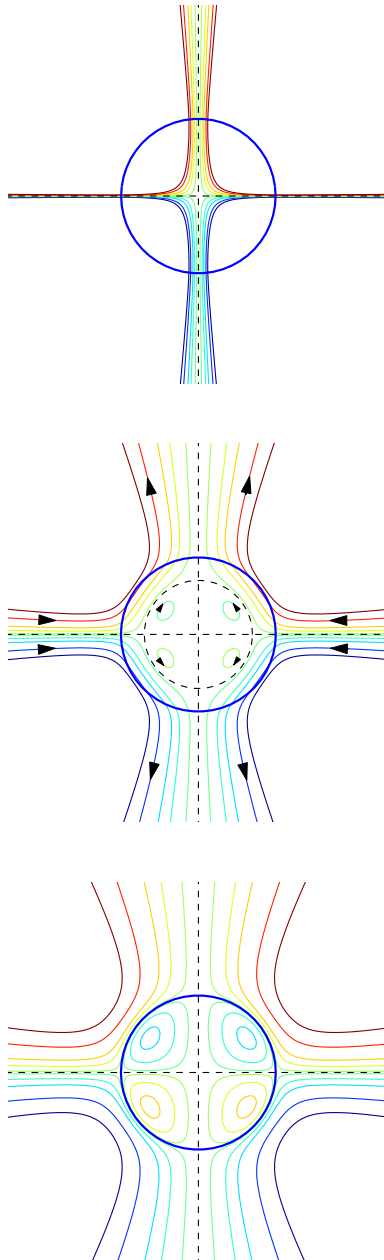


Figure 3: Evolution of the streamlines for a fluid system chosen from region (III) of the circulation-deformation map. Here, $R = 29.8$, $S = 2.27$, $\tilde{\mu} = 0.54$, and $Oh = 51.6$.

However, further inward motion of the initially extended vortices make the dividing streamline and the counterpart (extended) vortices visible (frame *c*). As time progress, the closed vortices are eventually confined inside the drop and the dividing streamline resides at the surface of the drop (frame *c*). At steady state, the sense of fluid flow is the same as the pertinent one depicted in Fig. (2). Furthermore, the drop deforms to a prolate.

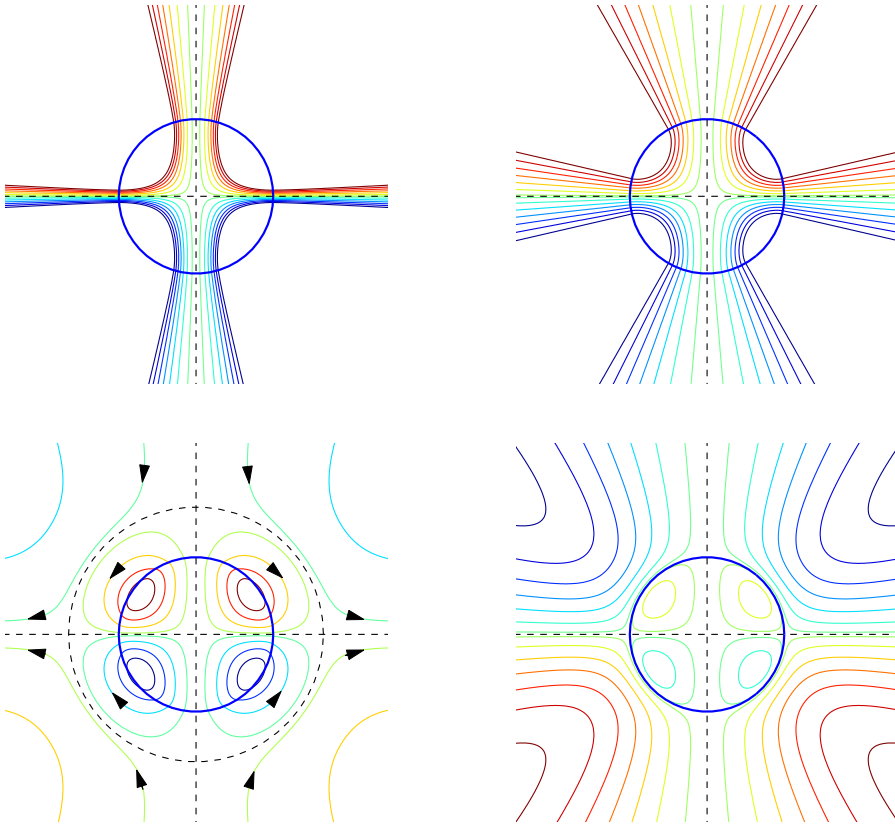


Figure 4: Evolution of the streamlines for a fluid system chosen from region (II) of the deformation map. Here, $R = 0.033$, $S = 0.1$, $\tilde{\mu} = 0.54$, and $Oh = 51.6$. The steady state deformation parameter is $\mathcal{D} = 4.3 \times 10^{-4}$. The times are $t = 0, \tau, 2.2\tau$, and 5τ . The time proceeds from left to right and top to bottom.

3 Discussion

To explore the reason for the observed differences, we examine the possibility of formation of the separatrix in the drop ($j = i$) and the ambient ($j = o$) by setting

$f_j(r) = 0$ in the expressions for the streamfunction $\psi_j = f_j(r) \sin^2 \theta \cos \theta$ ($j = i, o$); i.e., Eq. (11) and (12) of Esmaeeli and Sharifi (2011).

We first consider the streamfunction inside the drop. Setting $f_i(r) = 0$ leads to three roots, however, only one of them can possibly represent the radius of the circle $0 \leq r_{s_i} \leq 1$ that constitutes the separatrix

$$r_{s_i} = a \left[\frac{A_i + B_i \exp(-t/\tau)}{A_i + C_i \exp(-t/\tau)} \right]^{1/2} \equiv a\Lambda_i, \tag{2}$$

where

$$A_i = -\frac{3}{5} \left(\frac{19\tilde{\mu} + 16}{\tilde{\mu} + 1} \right) \frac{\Phi_t}{\Phi}, \quad B_i = \frac{16\tilde{\mu} + 19}{2\tilde{\mu} + 3}, \quad C_i = 3, \quad \Phi_t \equiv R - S.$$

In region (II), $\Phi_t/\Phi < 0$ according to Fig. (2) and, therefore, $A_i > 0$. Since $B_i > C_i > 0$ always, then $\Lambda_i > 1$ at all times. This implies that it is impossible to have a separatrix inside the drop. For regions (I) and (III), $\Phi_t/\Phi > 0$ according to Fig. (2) and, therefore $A_i < 0$. Thus, we need to evaluate the various possibilities concerning the signs and magnitudes of $N_i \equiv A_i + B_i \exp(-t/\tau)$ and $D_i \equiv A_i + C_i \exp(-t/\tau)$. Since $B_i > C_i > 0$, then N_i is always greater than D_i . However, we cannot draw a definite conclusion regarding the signs of N_i and D_i . Three possibilities exist: (1) if $[N_i < 0, D_i < 0]$, then $\Lambda_i \equiv \sqrt{N_i/D_i} < 1$ for all times. Therefore, there exists a dividing streamline inside the drop at $t = 0$; (2) if $[N_i > 0, D_i < 0]$ or (3) $[N_i > 0, D_i > 0]$, then the dividing streamline does not exist initially but it can form at some later time with infinitesimally small radius ($r_{s_i} \rightarrow 0$):

$$t_{0_i} = \tau \ln \left[\frac{5}{3} \frac{(16\tilde{\mu} + 19)(\tilde{\mu} + 1)}{(19\tilde{\mu} + 16)(2\tilde{\mu} + 3)} \frac{\Phi}{\Phi_t} \right]. \tag{3}$$

Here, $dr_{s_i}/dt > 0$ and, therefore, the radius of the dividing streamline increases monotonically until it resides at the surface of the drop, supporting the observation (seen in Fig. (3)) that the toroidal vortices will be formed inside the drop and then grew outward to occupy the drop.

Turning our attention to the streamfunction for the ambient flow and setting $f_o(r) = 0$ yields the radius of the circle $r_{s_o} \geq 1$ that can possibly represent the separatrix:

$$r_{s_o} = a \left[\frac{A_o + B_o \exp(-t/\tau)}{A_o + C_o \exp(-t/\tau)} \right]^{1/2} \equiv a\Lambda_o, \tag{4}$$

where

$$A_o = \frac{\Phi_t}{\Phi}, \quad B_o = \frac{5(3\tilde{\mu} + 2)(\tilde{\mu} + 1)}{(2\tilde{\mu} + 3)(19\tilde{\mu} + 16)}, \quad C_o = \frac{5}{3} \frac{\tilde{\mu} + 1}{2\tilde{\mu} + 3}.$$

Here the analysis is straightforward for regions (I) and (III), where $A_o > 0$ and $C_o > B_o > 0$ (always). Then, $\Lambda_o < 1$ at all times, which implies that it is impossible to have a dividing streamline in the ambient flow for these two regions. For region (II), we need to evaluate the various possibilities concerning the signs and magnitudes of $N_o \equiv A_o + B_o \exp(-t/\tau)$ and $D_o \equiv A_o + C_o \exp(-t/\tau)$ since $\Lambda_o < 0$. Three possibilities exist: (1) if $[N_o < 0$ and $D_o < 0]$, then $\Lambda_o = \sqrt{N_o/D_o} > 1$ and there exist a dividing streamline outside the drop at $t = 0$ with finite radius; if (2) $[N_o > 0$ and $D_o < 0]$ or (3) $[N_o > 0$ and $D_o > 0]$, then the dividing streamline does not exist at the beginning of the evolution but it will form at some later time far away (i.e., $r_{s_o} \rightarrow \infty$) from the drop:

$$t_{0_o} = \tau \ln \left[\frac{5(\tilde{\mu} + 1)}{3(2\tilde{\mu} + 3)} \frac{\Phi_t}{-\Phi} \right] \quad (5)$$

Here $dr_{s_o}/dt < 0$ and, therefore, the radius of the dividing streamline decreases monotonically until it resides at the surface of the drop, supporting the observation (seen in Fig. (4)) that the originally extended vortices gradually transform to closed vortices and move into the drop.

From the analysis so far, it is clear that the evolution of the flow field is closely related to the formation of the dividing streamline. As such, understanding the underlying mechanism behind the formation of the dividing streamline will be helpful in predicting the flow evolution. Here we lay out a methodology that is based on physical reasoning and can be used to analyze the current problem as well as the more complex circumstances where mathematical reasoning will be tedious. To this end, we note that the drivers behind the fluid flow (as well as the drop deformation) during the transient are the net normal and tangential electric stresses, $[[\tau_{rr}^e]]$ and $[[\tau_{r\theta}^e]]$, as given by Eq. (9) and (10) of Esmaeeli and Sharifi (2011), where the double bracket denotes the jump in a physical parameter at the surface of the drop. Since the sense of fluid flow driven by the individual stresses ($[[\tau_{r\theta}^e]]$ and $[[\tau_{rr}^h]]$) can be figured out qualitatively, the superposition of the two flow fields can help to understand the overall flow pattern; i.e. $\mathbf{u} \sim \mathbf{u}_t + \sim \mathbf{u}_n$. Here we denote the flow due to $[[\tau_{r\theta}^e]]$ and $[[\tau_{rr}^h]]$ as the shear- and the deformation-driven flows, respectively. During the transient, the senses of the shear- and deformation-driven flows are determined by the signs of $\Phi_t = R - S$ and $\Phi_n = \Phi - \Phi_t$, respectively, and their strengths are proportional to $|\Phi_t|$ and $|\Phi_n|$, respectively [Esmaeeli and Sharifi (2011)]. Furthermore, the shear-driven flow pattern for all the fluid systems is similar to the flow pattern seen for region (III) in Fig. (3)*b*, with the exception

that the senses of the flow for fluid systems chosen from regions (I) and (II) will be the opposite to that depicted in this panel. Similarly, the deformation-driven flow pattern will be similar to Fig. 3(a) or 4(a), except that the streamlines will be more bent. Thus, for fluid systems chosen from regions (II) and (III), where the drop is deformed to a prolate, the initially extended vortices cross into the drop at the equator and exit at the poles. Conversely, for a fluid system chosen from (I), where the drop deforms to an oblate, the direction of the flow is the opposite. To examine the results of the superposition of the shear- and deformation-driven flow patterns, rather than considering the whole flow field, we focus on the superposition of a representative streamline from each flow along the north pole. This makes the analysis much simpler and is valid since the dividing streamline is circular. We further note that along the dividing streamline the radial component of the velocity u_r is zero. Thus, the dividing streamline will form whenever the radial velocity vanishes because of the superposition of the two flow fields; i.e., $u_{r_t} + u_{r_n} = 0$.

Inclusion of $\Phi_n = 0$ in Fig. (2) makes the circulation-deformation map well-suited for transient flows. This leads to division of region (I) to a big (I_b) and a small (I_s) region, but does not affect the structure of regions (II) and (III). Here four possible senses of flow patterns and drop deformation exists according to the signs of Φ_t and Φ_n . Fig. (5) shows schematically the radial components of the shear-driven and the deformation-driven velocities; u_{r_t} and u_{r_n} , respectively. The analysis is relatively simple for regions (III) and (I_b). For these regions, the senses of shear-driven and deformation-driven flows are the same in the ambient fluid and, therefore, there is not a possibility for the formation of a dividing streamline there. However, the direction of the Φ_n -driven velocity is the opposite to that of the Φ_t -driven velocity in part of the drop. Thus, it is possible for a dividing streamline to form in the drop, as a result of competition of the opposing streamlines. This is in line with the mathematical derivation. On the other hand, for regions (II) and (I_s) the directions of the Φ_n -driven and Φ_t -driven velocities are the opposite both in the ambient and part of the drop. This suggests that there is a possibility of formation of a dividing streamline both in the ambient and the drop. This observation seems in contradiction with the results of the mathematical derivation where we showed that for regions (II) and (I) the dividing streamline is either possible in the ambient or the drop, respectively. This apparent discrepancy can be resolved easily considering the following facts. First, inside the drop, the dividing streamline will exist if the Φ_n -driven radial velocity is sufficiently weak so that it will only nullify “part” of the opposing Φ_t -driven radial velocity or it does not nullify it at all. On the other hand, if Φ_n -driven radial velocity is sufficiently strong so that it nullifies the “whole” opposing Φ_t -driven radial velocity, the dividing streamline will be pushed out from

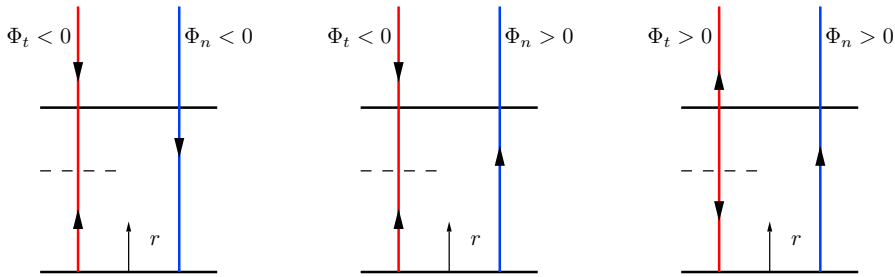


Figure 5: A schematic figure depicting the superposition of the shear-driven (Φ_t) and deformation-driven (Φ_n) flows along the north pole. The first and third frames correspond, respectively, to the flows in regions (I_b) and (III), and the second frame corresponds to the flow in regions (I_s) and (II). The lower and the upper horizontal lines represent, respectively, the z coordinates of the center and the surface of the drop and the dashed line shows the position of the dividing streamline in the shear-driven flow.

the drop into the ambient. Inspection of Fig. (2) shows that this is indeed what is happening in region (II). For this region, $|\Phi_n|$ is dominant over $|\Phi_t|$ since here the fluid velocity, running from the poles to the equator, tends to deform the drop to an oblate but the drop actually deforms to a prolate. Considering the fact that $|v_{r_n}| \sim |\Phi_n|$ and $|v_{r_t}| \sim |\Phi_t|$, then $|v_{r_n}|$ can override $|v_{r_t}|$, pushing the dividing streamline into the ambient. On the other hand for region (I_s), $|\Phi_n|$ is weak since it tends to deform the drop to a prolate, but the drop actually deforms to an oblate. Thus, for this region, $|v_{r_n}|$ can at most nullify part of the opposing $|v_{r_t}|$, leading to possible displacement of the dividing streamline in the drop.

4 Conclusion

The results of this study showed that for fluid systems in regions (I) and (III) the flow is established by formation of four vortices inside the drop that gradually grow outward until their growth is limited by the drop surface. On the other hands, for fluid systems in region (II) the steady state flow field is established through the evolution of four vortices that are formed in the ambient fluid and gradually penetrate into the drop until they are confined within the drop. The results of the qualitative analysis of the flow field by superposition of the shear-driven and deformation-driven streamlines showed that the predictions were in line with those of the mathematical derivation. This is encouraging, since for more complex flows where the mathematical reasoning becomes more difficult, the superposition technique will likely to be an effective means for prediction of the flow pattern.

References

- Christov, C.; Homsy, G.** (2009): Enhancement of transport from drops by steady and modulated electric fields. *Physics of Fluids*, vol. 21, no. 8, pp. 083102.
- Esmaeeli, A.; Sharifi, P.** (2011): Transient electrohydrodynamics of a liquid drop. *Phys. Rev. E*, vol. 84, pp. 036308.
- Halim, M. A.; Esmaeeli, A.** (2013): Computational studies on the transient electrohydrodynamics of a liquid drop. *FDMP: Fluid Dynamics & Materials Processing*, vol. 9, no. 4, pp. 435-460.
- Taylor, G.** (1966): Studies in electrohydrodynamics: I. the circulation produced in a drop by an electric field. *Proc. Roy. Soc. A.*, vol. 291, pp. 159-167.
- Vizika, O.; Saville, D. A.** (1992): The electrohydrodynamic deformation of drops suspended in liquids in steady and oscillatory electric fields. *Journal of Fluid Mechanics*, vol. 239, pp. 1-21.